Journal of Sustainable Development of Energy, Water and Environment Systems

http://www.sdewes.org/jsdewes

Year 2025, Volume 13, Issue 4, 1130622

Original Research Article

Maximum Power Point Tracking Based Solar Powered Hybrid System of Constant Speed Induction Motor and Electrical Load under Partial Shading Condition using Priority Based Modelling

Nouman Ashraf[1], Zeeshan Rashid[2], Ghulam Amjad Hussain*[3], Usman Humayun[4], Farrukh Hafeez[5], Zeeshan Ahmad Arfeen[2], Farhan Malik[6]

[1]Department of Renewable Engineering, MEENA Consultancy and General Contracting DMCC, Dubai, United Arab Emirates
e-mail: noumanashraf441@gmail.com

[2]Department of Electrical Engineering, The Islamia University of Bahawalpur, Bahawalpur, Pakistan
e-mail: zeeshan.rashid@iub.edu.pk, zeeshan.arfeen@iub.edu.pk

[3]College of Engineering and IT, University of Dubai, Dubai, United Arab Emirates
e-mail: ghussain@ud.ac.ae

[4]Department of Computer Engineering, Bahauddin Zakariya University (BZU), Multan 60800, Pakistan
e-mail: usmanhumayun@bzu.edu.pk

[5]Department of Electrical Engineering, Jubail Industrial College, Jubail, Saudia Arabia
e-mail: hafeez_f@rcjy.edu.sa

[6]Department of Electro-mechanical Engineering Technology, Abu Dhabi Polytechnic, Abu Dhabi, United Arab Emirates
e-mail: farhan.malik@actvet.gov.ae

Cite as: Ashraf, N., Rashid, Z., Hussain, G. A., Humayun, U., Hafeez, F., Arfeen, Z. A., Malik, F., Maximum Power Point Tracking Based Solar Powered Hybrid System of Constant Speed Induction Motor and Electrical Load under Partial Shading Condition using Priority Based Modelling, J.sustain. dev. energy water environ. syst., 13(4), 1130622, 2025,
DOI: https://doi.org/10.13044/j.sdewes.d13.0622

ABSTRACT

The solar photovoltaic energy sources are becoming popular due to being cleaner, sustainable and cost-effective sources of electrical energy. Photovoltaic sources are being deployed widely worldwide for residential and commercial use. In this research, a unique methodology is explored by modelling a 3-phase induction motor drive system fed from a photovoltaic source via pulse width modulation based inverter. The pulse width modulation pulse width modulation inverter technology provides a convenient way to control the motor speed by varying either the modulation index or the frequency of the reference signal for. The modulation index control method achieves faster dynamic response by enabling direct voltage amplitude adjustment, allowing for rapid torque control without inducing flux variations, which results in settling times of 0.2 s for speed and 0.12 s for torque compared to the frequency-based method with settling times of slightly greater than 0.5 s. The drive is integrated with heating and lighting load through a boost converter to absorb the surplus power from photovoltaic so that the overall system runs at maximum power point condition. Furthermore, partial shading condition is applied to assess the speed response of the motor, being the primary motive of this paper which is observed to stay at a reference of 1700 rpm. The prioritization of the motor load is ensured by the system's design, where the motor is directly fed by the inverter with control algorithms tailored to run at a desired speed, while the boost converter connected to auxiliary loads (heating and lighting) operates on the surplus power, as regulated by the maximum power point tracking algorithm.

KEYWORDS

Photovoltaic systems, Sustainable development, Switching converters, Variable speed drives.

INTRODUCTION

This Deployment of renewable energy systems and sustainable development is highly demanded globally and will be a key factor to determine the growth of a country in the near future [1]. After the analysis of 71 developing and 40 developed nations, it was found that renewable resource exploration has led to great growth in sustainable development, as shown by a new study [2], [3]. Sustainable development is determined by three factors, i.e., environment, economy, and society, as shown in Figure 1. Renewable energy systems have a direct impact on them due to being cleaner, cost-effective, and directly/indirectly improving the living standards of the society [4]. Renewable energy systems have a significant contribution in providing electrical energy, which is greenhouse gas-free and protects the environment [5]. The successful implementation of renewable energy depends primarily on government regulations, political factors, economic stability, energy security, policy stability and public awareness [6].

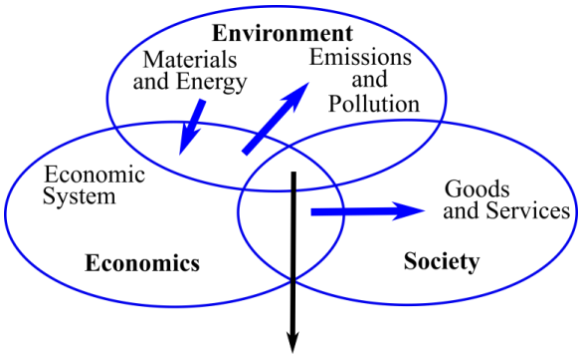

Figure 1. Factors for sustainable development

Multiple loads being used in villages rely on rotational movement, which are created by animals or pollution-causing diesel engines or heavy automobiles. Consequently, with ever-rising fuel prices across continents, such resources are slowly becoming non-feasible. One of the solutions to this problem is using a very powerful multi-purpose induction motor that can run at different speeds based on the type of load and gets powered from renewable energy sources such as solar photovoltaic (PV) technology. Solar radiation energy eliminates every conceivable operational complexity regarding power generation that is generally regarded as silent and non-polluting alternative source of electrical energy [7]. Because all the components and equipment required in the typical solar photovoltaic systems are static, they have minimal mechanical losses [8]. This makes them relatively more cost-effective and energy-efficient. Currently, solar power is facing various challenges, such as intermittency [9], maximum power point tracking (MPPT) [10], harmonics [11] as well as partial shading [12]; which makes research on it a priority among other RES.

The development of solar-powered induction motor drives has recently sparked an amazing step in the rapidly growing energy market for the generation of attractive revenues. Nam *et al*. suggested a sensor-less model predictive control (MPC) for the grid-connected inverter with inductor-capacitor-inductor (LCL) filter to minimize the total harmonic distortion (THD) to achieve real and reactive powers with minimum distortion [13]. A state estimator and a disturbance observer were designed as per Lyapunov stability theory to eliminate the need for sensors. The steady-state error was minimized by a cost function whose weights were effectively computed by using linear matrix inequality (LMI) for MPC. The authors also confirmed the effectiveness of the proposed controller through a linear quadratic regulator (LQR) and frequency response analysis with similar simulation results. Narendra *et al*. implemented a simulation framework for a reduced switch count-based inverter in PV fed single-stage induction motor for water pumping applications [14]. With four inverter switches, they successfully controlled voltage and speed using adaptive incremental conductance and direct vector control

methods, respectively. Rachaputi *et al*. reported similar work on single-stage sensor-less vector control of solar-fed induction motor drive for water pumping applications [15]. Their vector control approach incorporated three different maximum power extraction algorithms which gave a maximum power accuracy of >99.5% subjected to different partial shading conditions. The variations in voltage, current and speed were directly reflected in the PV output ensuring MPPT achievement in the presence of load thus making the product perfectly suitable for water pumping applications. Recently, Mounira *et al*. demonstrated speed control of PV-based doubly fed induction motor drive with sliding mode direct field oriented control method [16]. Under MPPT condition, they estimated the speed and flux of the motor based on Lyapunov's stability criterion using the observer in sliding mode. The research objectives in this relevant field are directed to standalone induction motor load under the successful implementation of MPPT in PV output but the problem mainly focused on control robustness. Kohlrusz *et al*. demonstrated changing possibilities of revolution by providing comparisons of two control strategies namely; scalar and vector control, based on real measurements done with no load, with direct current and with a locked rotor [17]. He concluded that the scalar control is rather cheaper and simpler at the cost of sluggish transient response compared to vector or field oriented (FOC) control. According to a review on direct and indirect FOC of induction motors by Gopal, FOC implementation is costly due to the presence of expensive flux sensors and furthermore, sensing is potentially inaccurate at lower rotor speeds [18].

This research work demonstrates the implementation of a PV-fed induction motor drive system and uses PWM-based inverter technology to provide a regulated AC power supply to the induction motor. This arrangement is aimed at regulating the speed and torque as per needs through simple command signals. The innovative part is that the speed control of the induction motor is done using scalar control without applying the constraint of maintaining the voltage-to-frequency ratio (*V/f*) constant. This constant *V/f* condition ensures fixed stator current and torque even after increasing or decreasing the motor speed at constant load. In this case, both current and torque are solely determined by the mechanical load. However, if the motor is kept in a safe operating mode where a slight increment in current doesn't hurt the winding, the motor speed can be regulated by either *V* or *f*, while keeping the other variable constant. In this case, the motor torque will be determined by two variables, namely load and *V* (or *f*) which will provide a faster response compared to the conventional scalar control method. Additionally, a resistive load at the output of a DC–DC converter is connected in parallel to the inverter/motor, making PV output feeding a hybrid (mechanical and electrical) load under MPPT condition.

The hybrid load operation demands the modeling of prioritization to rank the connection of load based on their requirement in emergency situation when the generation is limited. This scenario is mostly prevailed during renewable energy operation especially for PV working under partial shading condition (PSC). One recent approach used exhaustive search algorithm for implementing the load prioritization based on the time of operation during one day [19]. After repetitive execution of the search optimization, the priority scores are evaluated such that the user satisfaction gets closer to unity. Another expedient approach used autonomous fuzzy controller in the presence of demand response system, renewable energy management system and load forecasting module [20]. This approach requires information of ambient temperature, consumption time, tariff variation and renewable energy availability. This data is used altogether to obtain the consumer comfort level which is similar to user satisfaction which is maximized by the fuzzy controller. Another simple method is used by Rathod *et al*. which consists of running low and high priority loads by PV, battery and solid oxide fuel cell [21]. In this method, the low priority load is switched off during PV standby timing when fuel cell and battery are running the load. This work was done in the presence of MPPT phenomenon and the load scheduling was done solely by the closed loop control mechanism.

The current scenario also requires the involvement of load priority decision especially under PSC when a motor control command is already in place which is an aspect absent from the technical literature. Both electrical and mechanical loads are vulnerable to fluctuations in

PV output however; there remains one load which should work steadily owing to the nature of service. To maximize the efficiency of the system, MPPT is enforced over the operation of PV plant since the inherent efficiency of PV plant is quite low. It is notable that the motor running at fixed speed requires a constant operating power from PV source, due to which a surplus amount of power is available at the PV output which has to be transferred to some load to satisfy MPPT condition [22]. As a result, a switching-type boost converter with a resistive load can be integrated at the DC output of the PV plant to dissipate the surplus active power under MPPT operation [23]. The key idea behind this concept is to operate heating and lighting loads which are resistive in nature from the power left after the constant speed motor operation. The innovative part of this research is that if PSC occurs, the motor will continue its constant speed operation whereas the loss of power will be reflected in the boost converter output. The load priority goal is implicitly modeled solely based on the controller and filter gains in the system without the requirement of complex priority scheduling protocols [24].

The simulation test setup is built in the MATLAB/SIMULINK software, using a power system simulator module that encompasses all its components found in its database. The SIMULINK library itself contains switches, RES batteries, RLC components motors controllers and signal generators which were used in the model. In the first step, prototype simulations were carried out with a direct AC power source to assess the power consumption of the motor under different loading conditions. In this setup, the inverter was not involved. These power consumption values at this step are used as input variables for filter design when the same motor is driven by PV sources via an inverter. In the second step, a sophisticated control system is designed to modulate the tuning variable of the applied AC voltage to the induction machine which eventually regulates speed according to the target value. Speed regulation can be achieved either through modulation index or frequency as tuning variables while keeping other parameters constant so that meaningful comparisons can be made on speed response. Rotor speed (N_r) is measured by using a tachogenerator which is then compared with reference speed (N_{ref}) through a subtractor block as explained in **Figure 2**. The error signal is obtained from the subtractor block which is used as an input to a proportional integral (PI) controller whose proportional gain (K_P) and integral gain (K_I) are adjusted to achieve the desired amplitude and frequent of a 3-phase reference signal for PWM.

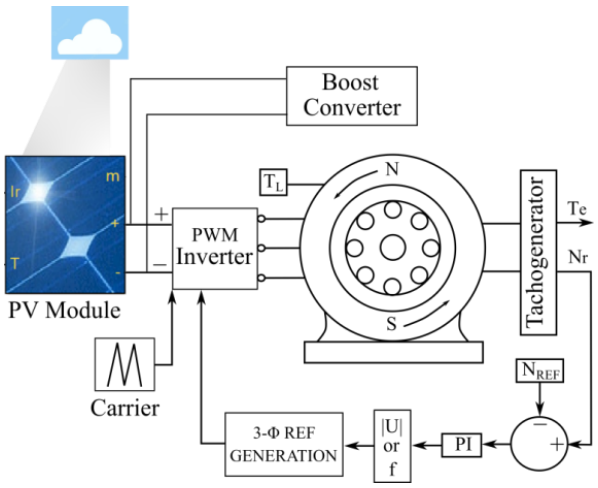

Figure 2. The schematic diagram of simulation test setup

The inverter that has been adopted in this model uses a sinusoidal pulse width modulation (SPWM) technology that is driven by a carrier signal of 1 V amplitude and a frequency of 10 kHz. This offers improved results than conventional methods in harmonic distortion. In this technique, a reference sine wave signal is compared with a triangular carrier signal to generate a pulse sequence whose width is maximum at the peaks of the sine wave and vice versa. Thus, instead of a constant duty cycle found in square wave inverters, sinusoidal duty cycles are used

to control inverter switches. Therefore, output pulses closely resemble sinusoidal waveforms; hence, small filter components can be used to reach certain levels of harmonic distortion so as to minimize their cost when building up the system [25].

Recent studies on PV fed induction motor drives have explored various control strategies to improve dynamic performance under variable solar conditions. For instance, Choudhary *et al*. investigated a PV-powered vector-controlled induction motor using a space vector PWM inverter, achieving a speed settling time of approximately 0.4 s under standard test conditions [26]. Similarly, Kumar and Agarwal implemented a direct torque control (DTC) scheme for a PV-fed motor and reported torque settling times in the range of 0.2 to 0.3 s, with enhanced stability during partial shading [27]. In another approach, Nahin *et al*. developed a model predictive control (MPC)-based PV motor drive system that demonstrated improved transient behavior with speed settling within 0.25 s and torque settling near 0.15 s [28]. These studies highlight the ongoing effort to achieve fast and stable responses in PV-powered motor systems, although most approaches rely on advanced control algorithms with higher computational requirements. Compared to these, the proposed modulation index-based control in our study achieves competitive settling times – 0.2 s for speed and 0.12 s for torque – while maintaining a simpler control architecture and operational robustness under partial shading.

PHOTOVOLTAIC PLANT WITH MAXIMUM POWER POINT TRACKING ALGORITHM

The simulation platform is furnished with PV plant "1Soltech 1STH-215-P" having 40 series and 40 parallel connected cells. With an irradiance of 1000 W/m^2, the plant features a short circuit current (I_{sc}) of 30.9 A, open circuit voltage (V_{oc}) of 1320 V and maximum power (P_{MPP}) of 339 kW. The corresponding values of all parameters under partial shading condition (PSC) of 500 W/m^2 and 200 W/m^2 are different and are illustrated in **Table 1**. The Soltech 1STH-215-P module was selected due to the following key characteristics that align well with the design requirements of our application:

- Moderate Power Rating (215 W): This allows for flexible scaling in modular configurations to meet the power demand of both the motor and auxiliary loads.
- Stable Output Characteristics: The module offers reliable performance under varying environmental conditions, which is crucial for maintaining steady power to the motor drive and supporting the boost converter operation.
- Widely Available Datasheet and Model Parameters: The module's specifications, such as short-circuit current, open-circuit voltage, and maximum power point voltage and current, are well-documented, enabling accurate simulation and modelling in MATLAB/SIMULINK.
- Compatibility with MPPT and Boost Converter Design: The module's voltage and current characteristics fit well within the operational range of the MPPT algorithm and boost converter used in our system design.

Table 1. PV plant variables at various irradiances

Irr. (W/m^2)	V_{oc} (V)	I_{sc} (A)	V_{MPP} (V)	I_{MPP} (A)	P_{MPP} (kW)
1000	1320	30.9	1155	292	339
500	1410	158	1169	145	171.7
200	1455	314	1119	30	32.10

The maximum possible efficiency from PV panels is confined which demands for using maximum power point (MPP). The key idea behind MPPT algorithm is estimating the voltage (V_{MP}) at which dP/dV is zero. There are several conventional algorithms including perturb and observe, parasitic capacitance and maximum voltage while this paper utilizes

the incremental conductance method [29], [30]. After all tracking algorithms have converged, the incremental conductance method settles at MPP, while other methods cause oscillations [31].

The control block containing an embedded MPPT algorithm was depicted in Figure 3, after generating a delay of 0.1 ms on the PV voltage and current signals (V_{PV} and I_{PV}). The 0.1 ms delay was intentionally introduced to prevent control loop instability and ensure robust convergence of the MPPT algorithm. Specifically, this short delay serves to avoiding high frequency oscillations, allowing settling time for converter response and offers improved algorithm stability. Without such a delay, the continuous and rapid updates to the duty cycle of the boost converter can cause high-frequency oscillations in both the voltage and current. The delay also gives the boost converter's output voltage sufficient time to respond to each new duty cycle command before the MPPT algorithm makes another adjustment.

The error signal received by the PI regulator is generated from V_{MP} which is deducted from V_{PV} by means of MPPT algorithm. A comparison between a sawtooth waveform and the output of the regulator provides a pulse sequence that operates an IGBT switch for the boost converter. It is worth mentioning that the regulator output gets constrained between 0 and 0.95 levels since sawtooth waveform changes between 0 and 1; thus, making it meaningful in terms of comparison with this regulator range. To reduce an error, a PI controller will also change the power control cycles in order to pull V_{MP} as near as possible to the operating voltage level. The saturation limit is constrained between 0 and 0.95 while the frequency of sawtooth waveform is used as 5 kHz.

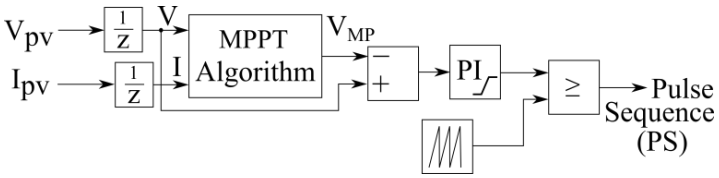

Figure 3. Pulse sequence generation for converter switching in MPPT operation

FILTER DESIGN FOR BOOST CONVERTER

In the discussed case, the machine consumes a constant amount of power lower than the MPP of the PV system while operating at constant speed and torque. For MPPT to occur, any excess power left after motor load should be dissipated into some passive component which is taken as a resistor in this study. However, this power cannot be simply dissipated; instead, it requires switching action so that the duty cycle remains at its optimum value such that when *VI* = constant. Even though any type of DC-DC converter may be used, a traditional boost converter has been selected for this purpose, which is connected in parallel with the driver circuit at PV output as shown in Figure 4. The values of the components used for the boost converter are: C_{sh} = 1000 μF, R_{sh} = 0.1 mΩ, C = 6.1 mF, L=8.2 mH, R_L = 16.24 Ω, V_o = 2300 V.

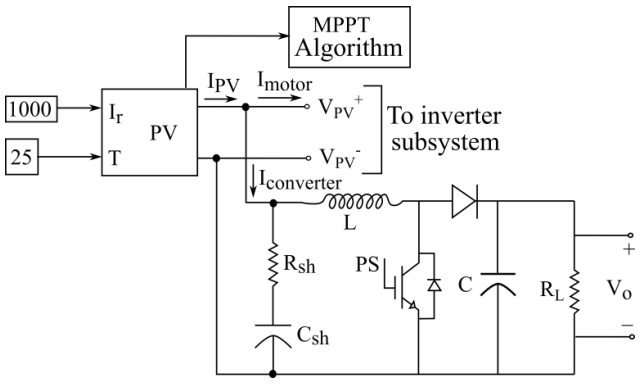

Figure 4. Schematic diagram of PV fed boost converter

The converter output possesses ripples which are minimized using a shunt capacitor connected in parallel with the load resistor. Before designing the LCR components of the filter, PV current (I_{PV}) and motor current (I_{motor}) are calculated using eqs. (1) and (2) respectively.

Eq. (3) calculates the apparent power drawn by the motor (S_{motor}) using P_{motor} (8.2 kW) and Q_{motor} (12.9 kVAR) which are measured at the input side of the motor. The converter current is given by the difference of I_{PV} and I_{motor} as shown in eq. (4).

$$I_{PV} = \frac{P_{PV}}{V_{PV}} \tag{1}$$

$$I_{motor} = \frac{S_{motor}}{V_{PV}} \tag{2}$$

$$S_{motor} = \sqrt{P_{motor}^2 + Q_{motor}^2} \tag{3}$$

$$I_{converter} = I_{PV} - I_{motor} \tag{4}$$

The values of LCR components are calculated assuming 5% ripples in I_{PV} and 0.1% ripples in output voltage of the converter (V_o) [see eqs. (5) and (6)]. The volt-ampere at the converter output is equal to the volt-ampere at the PV output minus the volt-ampere across the motor, which is used to calculate the output current (I_o) of the converter as given by eq. (7). Finally, the LCR values are given by eqs. (8) – (10).

$$\Delta I = 5\% \text{ of } I_{PV} \tag{5}$$

$$\Delta V = 0.1\% \text{ of } V_o \tag{6}$$

$$I_o = \frac{P_{PV} - S_{motor}}{V_o} \tag{7}$$

$$R = \frac{V_o}{I_o} \tag{8}$$

$$L = \frac{V_{PV}(V_o - V_{PV})}{f_{st} \times \Delta I \times V_o} \tag{9}$$

$$C = \frac{I_o(V_o - V_{PV})}{f_{st} \times \Delta V \times V_o} \tag{10}$$

BLOCK DIAGRAM FRAMEWORK OF MOTOR CONTROL

The output of the PV plant is further connected to the induction motor drive circuit, which is placed electrically parallel to the converter as can be observed in **Figure 4**. The drive circuit consists of (i) Control subsystem (SS), (ii) Inverter SS and (iii) Motor SS as shown in **Figure 5**. The Control SS generates and adjusts the 3-ϕ reference signal ($V_{abc,ref}$) in response to the difference between the desired and actual motor speeds. According to the PWM reference, Inverter SS generates 3-ϕ AC voltage (V_{abc}) from the DC voltage of the PV plant which is fed to the motor SS. Motor SS contains the 3-ϕ induction motor having a measurement setup for P_{motor} and Q_{motor} at the input side to be used in the filter design calculations. The motor output is

connected to a tachogenerator to measure the rotor speed (N_r). The measured N_r is fed back to the Control SS to maintain it close to the reference speed (N_{ref}).

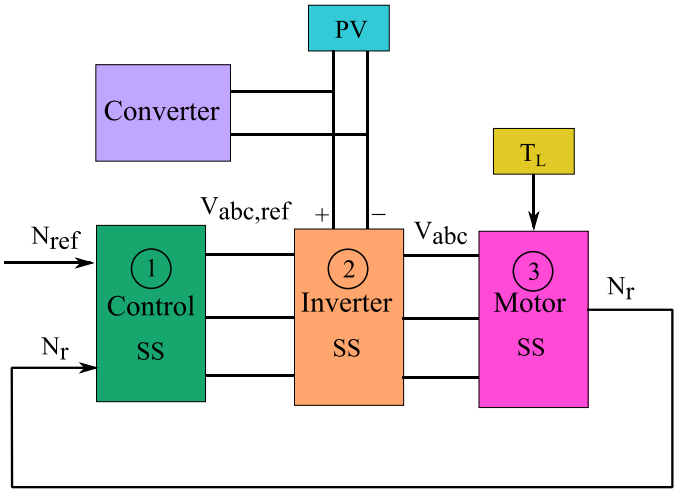

Figure 5. Three subsystems (SS) involved in the model

Control Subsystem

The speed of the induction motor varies directly with the amplitude and frequency of the applied AC voltage. These two electrical parameters are considered as control parameters for speed regulation to investigate the controller response and draw a fair comparison.

Modulation Index (*M*) Based Control. In the first case, frequency (*f*) is kept fixed at 60 Hz and output of the PI controller is treated as modulation index (*M*) which gets adjusted according to the speed error during the course of the simulation as shown in **Figure 6**. The triangular carrier signal in inverter SS has the amplitude of 1 so *M* is equal to the amplitude of $V_{abc,ref}$ ($|u|$).The proportional and integral gains (K_P and K_I) of PI controller are kept at 0.004 and 0.08, respectively. In this method, speed control is achieved by varying the modulation index at a fixed frequency. This approach affects the amplitude of the inverter output voltage, which in turn influences the motor torque more directly and linearly. Because modulation index changes result in faster and more predictable torque response, the system exhibits a more stable and responsive dynamic behavior with less phase lag. The system is naturally more responsive, so smaller gains are sufficient to achieve fast convergence and avoid overshoot or oscillations. Larger gains were found to make the system overly aggressive and prone to instability.

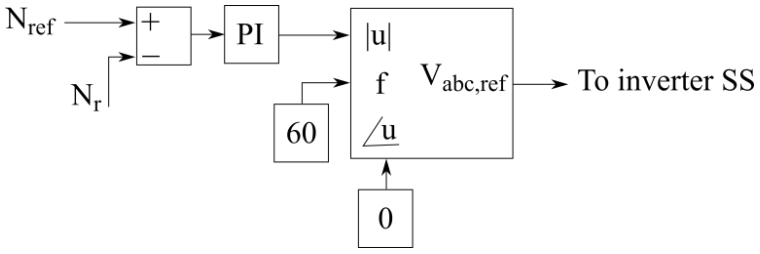

Figure 6. M-based Control SS with KP = 0.004, KI = 0.08

Frequency (*f*) Based Control. In the second case, |u| is kept constant at 0.59 whereas *f* is adjusted by PI controller (K_P= 0.008, K_I = 0.3) in proportion to the speed error signal coming from the subtractor block as shown in **Figure 7**. In this method, motor speed is controlled by varying the frequency of the reference signal. Changes in frequency affect both the magnetic flux and torque, introducing slower dynamics and higher time constants. The system becomes less sensitive to small changes in frequency and takes longer to respond, requiring higher PI

gains to compensate for this inertia and improve convergence speed. Larger K_P and K_I values are required to accelerate error correction and ensure satisfactory dynamic response. These gains help overcome the lag introduced by the frequency-dependent behavior of the motor.

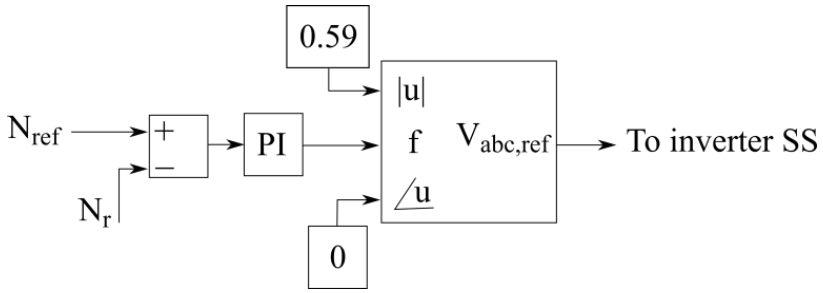

Figure 7. f-based Control SS with KP = 0.008, KI = 0.3

PWM Reference Generation. With phase kept at 0, $|u|$ and f signals are fed to the 3-ϕ reference generation block (shown in **Figure 8**) whose output ($V_{abc,ref}$) is sent to the Inverter SS. The f value is first converted to ω by multiplying with 2π and then subsequently integrated to obtain ωt which is the argument of sinusoidal reference. Three phase shift vectors equal to 0, $-2\pi/3$ and $2\pi/3$ are initialized and added to ωt to generate 3-ϕ signals separated by 1200. Finally, the sin function is executed over the three vectors and $|u|$ is multiplied with it to obtain $V_{abc,ref}$. In M-based control, $V_{abc,ref}$ has constant f of 60 Hz whereas $|u|$ varies according to the speed command. In f-based control, $|u|$ remains constant at 1 and f varies which will be observed in the next section.

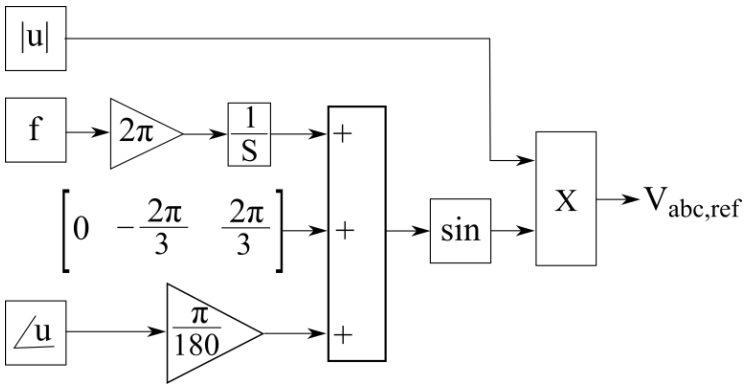

Figure 8. 3-phase reference generation block

Inverter Subsystem

Inverter SS receives $V_{ref,abc}$ signals with unique amplitude and frequency from Control SS which are compared with single carrier signal using logical operator as shown in **Figure 9**. The carrier signal is a triangular repeating sequence with amplitude (V_c) of 1 V and a frequency (f_c) of 1 kHz. The choice of a 1 kHz triangular carrier frequency for the PWM inverter was made based on a balance between system response requirements, switching losses, and simulation efficiency. In practical motor drive systems, switching frequencies between 1 kHz and 5 kHz are commonly used depending on the motor rating and inverter design. The comparator output contains pulses (0 or 1) which are labeled as PWM_1 and this signal is complemented using a NOT gate to generate PWM_2 and so on. These PWM pulses are fed to the gate terminals of the IGBT switches of the inverter.

Due to complement operation, both switches across one leg cannot turn on simultaneously, preventing short circuit at the PV terminals. It is notable that the PWM inverter generates AC voltage with the same frequency as that of $V_{abc,ref}$ and its amplitude varies directly from that of $V_{abc,ref}$.

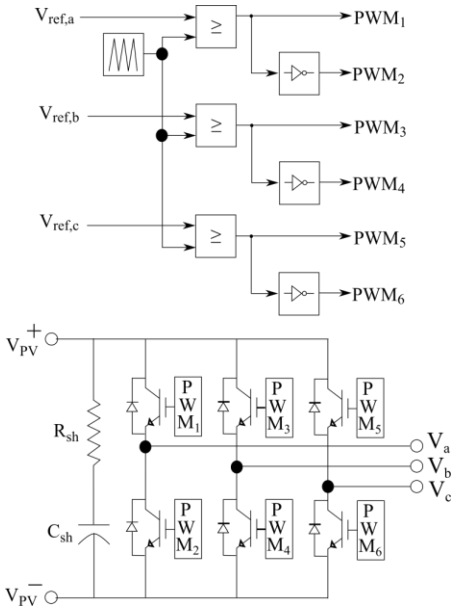

Figure 9. 3-ϕ PWM inverter: Vc = 1 V, fc = 1 kHz, Rsh = 1 mΩ, Csh = 500 μF

Motor Subsystem

The Motor SS contains a 4 pole, 5 hp, 460 V, 60 Hz, having a typical speed of 1750 rpm with other parameters summarized in **Table 2**. Motor SS receives 3-ϕ AC signal from Inverter SS with a power measurement block, and it also inputs the load torque (T_L) which is fixed at 40 Nm as shown in **Figure 10**. The chosen outputs of the motor for analysis purposes are (N_r) and rotor mechanical torque (T_r) using the bus selector.

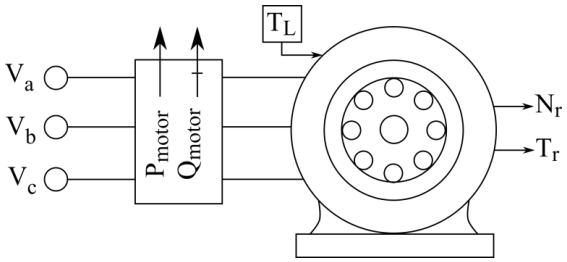

Figure 10. 3-ϕ induction motor with power measurement block, TL = 40 Nm.

Table 2. Specifications of induction motor used

Parameter	Value	Parameter	Value
Maximum output power	5 hp	Voltage	460 V (*L-L*)
f	50/ 60 Hz	Rated speed	1750 rpm at 60 Hz
R_1 (Stator resistance)	1.15 Ω	R_2 (Rotor resistance)	1.10 Ω
L_1/L_2 (Stator/rotor inductances)	5.97 mH/5.97 mH	No. of poles	4

RESULTS AND DISCUSSION

The comprehensive simulation infrastructure presents a wide spectrum of results and analysis for *M* and *f*-based control strategies which are discussed in parallel for one-to-one comparison. In the first phase, only the motor is fed from the PV and its speed/torque are plotted on top of their respective reference/load values to see the control action. Second phase deals with the MPPT operation of the PV plant, which is achieved by adding a boost converter at the PV output in parallel with the motor. Finally, PSC is applied at the PV plant, and the

speed control objective, as well as the power dissipation across the converter load is analyzed. These scenarios are subsequently discussed in the following subsections.

Response of Photovoltaic Fed Motor

The speed and torque response of the induction motor without converter integration is plotted in **Figure 11a** and **Figure 11b** respectively for *M*-based control. N_{ref} is selected as 1400 rpm, 1700 rpm and 1550 rpm for 0.5 s each whereas T_L is fixed at 40 Nm as shown by black lines. The motor undergoes a swift response with N_r settling at all values of N_{ref} and T_r also following T_L. As N_{ref} changes, the motor shows some oscillation in T_r however, these oscillations are minor and short-lived corresponding to small jerks. In *f*-based control, the motor takes longer to settle at N_{ref} and oscillations in T_r are also relatively longer, as shown in **Figure 11c** and **Figure 11d**. In the first 0.5 s, N_r stays in oscillating mode while converging at N_{ref} since the motor starts from rest however, from t = 0.5 – 1 s and 1 – 1.5 s, the motor slowly settles at N_{ref}. When the controller alters the supply frequency, synchronous speed (rpm of the stator magnetic field) increases which increases rate of change of flux, induced emf and torque to set the motor at the new speed after a series of these phenomena making it quite a slow process. The controller sensitivity is however, quite high which does not wait too long to check the final steady speed of the rotor and goes on increasing the frequency, due to which speed goes beyond the reference value and controller has to decrease the frequency again. Due to this reason, more oscillations are observed in speed and torque of the motor as can be seen in **Figure 11c** and **Figure 11d**. From the torque's point of view, there are longer oscillations at the start which diminish when the motor settles and these oscillations are negligible at the transition time of N_{ref} as opposed to the *M*-based control case. From this discussion, it is evident that the response time in *M*-based control is superior and the motor is more sensitive to the command changes and in *f*-based control, motor starts with a sluggish response, but the torque fluctuations in running condition are negligible.

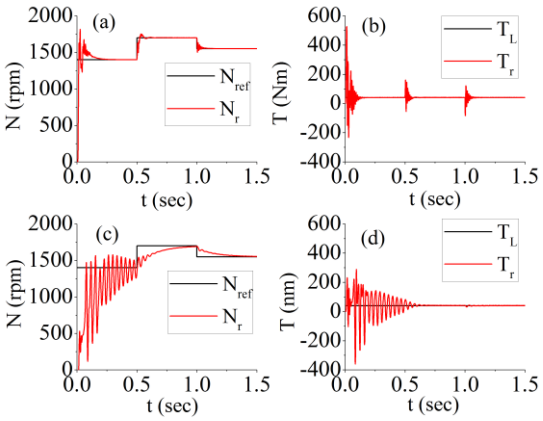

Figure 11. 3-ϕ induction motor with power measurement block, TL = 40 Nm

The tuning response of *M* and the resultant $V_{abc,ref}$ are plotted in **Figure 12a** and **Figure 12b**, respectively for the *M*-based speed control case. For the three values of N_{ref} during each 0.5 s interval, the corresponding value of *M* changes in a direct proportion which modifies the amplitude of PWM reference. In this case, *f* is kept constant at 60 Hz which can be observed in a uniform color pattern of $V_{abc,ref}$ in **Figure 12b**. On the other hand, the *M* is constant but *f* is modified in response to the speed error which can be observed in different color patterns along $V_{abc,ref}$ signal in **Figure 12d**. Furthermore, in *f*-based control, settling of *f* variable is comparatively slower as compared to *M* in the previous case where sharp correction in modulation index is observed. This slow tuning of *f* is attributed to sluggish or lagging behaviour of motor in response to the frequency of the AC input. An attempt to speed up the controller response by varying the gains causes the motor to go in longer oscillations which is a

case of poor control performance. As a result, the settling time as well as the total harmonic distortion of the speed and torque response will further increase.

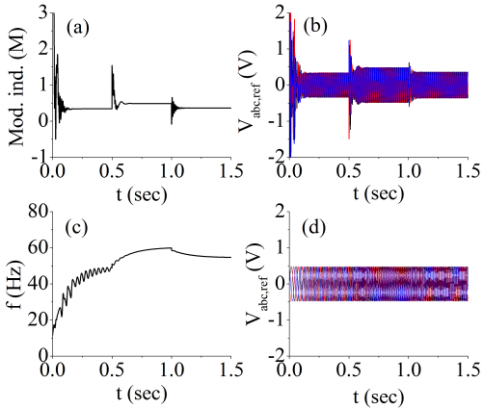

Figure 12. Plots of: a) M and b) Vabc,ref in M-based control; plots of: c) f and d) Vabc,ref in f-based control

Response of Converter Integrated Photovoltaic Fed Motor under Maximum Power Point Tracking

MPPT can be realized using any kind of switching converter, though this study mainly employs a boost converter with a resistive load. Both the N_r and M have been plotted in **Figure 13a** and **Figure 13b** for the integrated converters discussed. Due to the slowness of MPPT operation in relation to speed tracking objective, it increased time for simulation up to 3.5 seconds. In this case, N_r got incremented at the start of the simulation beyond N_{ref} and then settled down in the same way as M; nevertheless, then MPPT took some considerable amount of time before attaining a steady state.

When designing, 2300 V is selected as the converter output (V_{DC}), and the P_{MPP} of the chosen plant is 339 kW. The steady-state values of V_{DC} and P_{PV} are seen to settle at the desired values, as shown in **Figure 13c** and **Figure 13d** respectively. These plots illustrate that motor speed control goal has been achieved with the extra generated power going into the converting devices' ohmic loads. It is noteworthy to point out that, although the MPPT phenomenon is quite slow being settled at around 2.5 s, yet the speed response of the motor is quick which reaches the steady state at 0.61 s. The same quick settling is also observed in M as can be seen in **Figure 13b**.

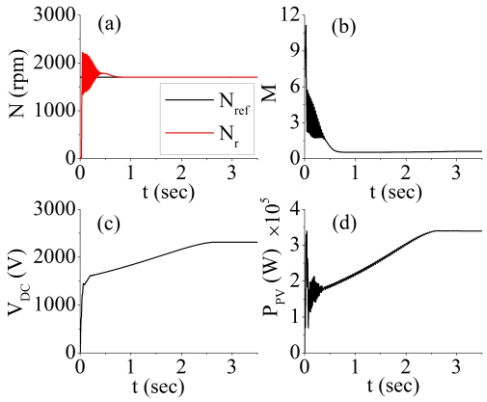

Figure 13. Plots of: a) Nr; b) M; c) VDC and d) PPV in M-based control under MPPT

Figure 14 illustrates the response of the same quantities for *f*-based control where speed tracking response is plotted right next to the f variation as the solver progresses. After considerable oscillations, N_r settles to N_{ref} successfully as shown in **Figure 14a** as a result of

correct frequency tracking and stabilization presented in **Figure 14b**. The converter output is depicted in **Figure 14c** where a nice settlement of V_{DC} at 2300 V with a nice filtration process can be observed. Moreover, P_{PV} is plotted in **Figure 14d** which shows that MPPT operation is successfully accomplished during simulation duration of 3.5 s. Similar to the previous case, the N_r and f responses are faster and they are independent of the convergence behaviour of MPPT algorithm whose effect is solely reflected in the boost converter output.

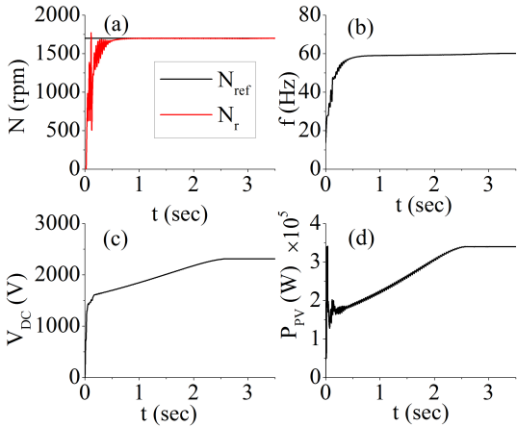

Figure 14. Plots of: a) Nr; b) f; c) VDC and d) PPV in f-based control under MPPT

Response of Converter Integrated Photovoltaic Fed Motor under Maximum Power Point Tracking and Partial Shading Condition

The last set of outcomes concerns the working of a motor integrated with a converter system under both situations of MPPT and PSC. It is noteworthy that the motor runs in a closed loop to control its speed while there is no feedback for voltage or current regulation within the converter. Therefore, to keep its speed constant during PSC, it will first draw power from the PV plant before dissipating any surplus into the converter load which will experience a dip after PSC. The response of N_r and M for M-based control of the motor are demonstrated in **Figure 15a** and **Figure 15b**, respectively; with a PSC applied at the middle of the simulation run lasting 3.5 s (irradiance equals 500 W/m^2). A slight fluctuation is observed in N_r at 3.5 s due to a drop in PV power that forces PI controller associated with speed control loop to raise M so that the inverter voltage of all the three phases and hence N_r can be reverted back to its initial value which is 1700 rpm. On the other hand, converter output (V_{DC}) undergoes a dip as a result of PSC which coincides with overall reduced power generation to MPPT equal to the new 172 kW (see **Table 1**) indicated **Figure 15d**. The fluctuation in speed response of the motor is small and abruptly healed whereas the converter output stabilizes slowly due to the sluggish nature of the MPPT algorithm.

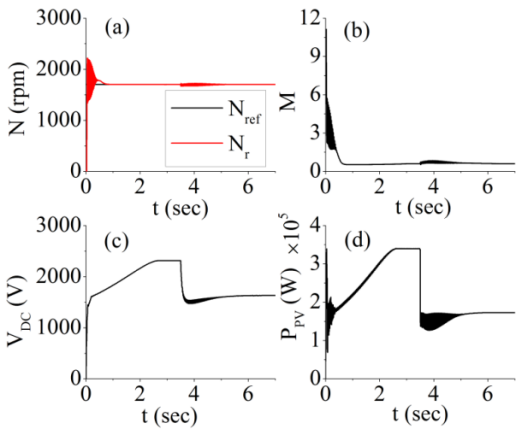

Figure 15. Plots of: a) Nr; b) M; c) VDC and d) PPV in M-based control under MPPT and PSC

Figure 16 illustrates the system response under PSC after t = 3.5 s for f-based control. The behavior of N_r can be observed in **Figure 16a** on top of N_{ref} which shows that successful speed tracking has been achieved. At the instant of PSC, slight oscillations are observed in N_r due to the availability of reduced power from PV which is compensated by an equivalent rise in the frequency as shown in **Figure 16b**. The effect of PSC is solely reflected in the converter output power causing a substantial decrease in V_{DC} as shown in **Figure 16c** whereas the motor is still running at the same mechanical power. The initial designated value of V_{DC} is 2300 V which is reduced to 1629 V as a result of PSC. The PV plant is shifted to a new MPP which is 172.8 kW as a result of PSC implying the successful convergence of the tracking algorithm as illustrated in **Figure 16d**. From all the sets of simulation exercises, it is evident that both M and f-based control methods are adequately designed and modeled in SIMULINK such that all the set parameters conform to the successful control tasks.

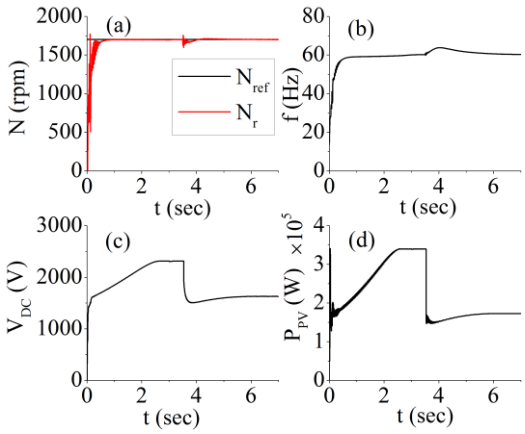

Figure 16. Plots of: a) Nr; b) f ; c) VDC; d) PPV in f-based control under MPPT and PSC

Table 3 summarizes the overall responses of control variables (N_r and T_r), tuning variables (M and f), converter output (V_o) and PV power. In the M-based control, the responses of N_r and T_r are fast and smooth whereas in f-based control, these responses are observed to be slow and oscillatory both in full irradiance and PSC. The same behavior is found in the tuning variables for both irradiance conditions. On the other hand, V_o response is observed to be slow with small oscillations in only PSC and in M-based control whereas this variable's response is slow and smooth for all other conditions. Finally, the tracking response of PV power is also found to be slow, with small oscillations in full irradiance and oscillatory in PSC for both control methods.

Table 3. Summary of responses of control variables, tuning variables, converter output and PV power tracking

Parameter	Irradiance	*M* based control	*f* based control
N_r/T_r response	Full	Fast, smooth	Slow, oscillatory
	PSC	Fast, smooth	Slow, oscillatory
Tuning variable	Full	Fast, smooth	Slow, oscillatory
	PSC	Fast, smooth	Slow, oscillatory
Converter output	Full	Slow, smooth	Slow, smooth
	PSC	Slow, small osc	Slow, smooth
MPP tracking	Full	Slow, small osc	Slow, small OSC
	PSC	Slow, oscillatory	Slow, oscillatory

The efficiency of the whole system and the THD values for different cases of simulation study are summarized in **Table 4**. The modes of operation considered in this work are (i)

induction motor control fed with PV, (ii) induction motor control fed with PV under MPPT and (iii) induction motor control fed with PV under MPPT and PSC. In all these modes of operations, both *M* and *f*-based control methods are implemented. The system efficiency is evaluated by dividing the total (mechanical and electrical) output power with the maximum power of the PV plant. The THD values are obtained by simply connecting the built-in THD block of SIMULINK at the output response (in parallel with the scope). For the first case, THD values are found to be 1.35% and 1.21% whereas the efficiencies are evaluated to be 39% and 29% for *M* and *f*-based control methods respectively. For the second case, THD values are recorded as 1.19% and 1.23% whereas efficiencies are found as 91% and 89% for the two control methods. Clearly, the efficiency is maximum in this case of MPPT operation since maximum power is fetched from the PV. In the third case, THD values are evaluated as 1.12% and 1.15% and efficiency values are found as 82% and 78% which are slightly smaller due to the less generation in PSC. In all cases, the THD values in the converter output are smaller than 1.5% which is the maximum allowable limit declared by the IEEE standard 519-2022 **[32]**.

Table 4. Summary of efficiency and THD for various operation modes

Mode of operation	Control	THD	Efficiency
PV fed motor	*M*	1.35%	39%
	f	1.21%	29%
PV fed motor under MPPT	*M*	1.19%	91%
	f	1.23%	89%
PV fed motor under MPPT and PSC	*M*	1.12%	82%
	f	1.15%	78%

FEASIBILITY OF THE PROPOSED SYSTEM AND LIMITATIONS

The economic feasibility of the proposed PV-powered motor drive system is promising, particularly in off-grid or weak-grid rural regions. While the initial capital investment includes the cost of PV modules, a PWM inverter, boost converter, and control circuitry, these are offset by minimal operational costs, low fuel dependency, and long equipment lifespan. The selected Soltech 1STH-215-P module is relatively cost-effective and widely available, making it suitable for decentralized applications.

The proposed control system is observed to be robust, error free, noise free and faster even for running the induction motor whose circuit is inductive with slow transient times. In a relevant contemporary published article, PV and multilevel inverter fed induction motor along with buck-boost converter is designed for speed control application **[33]**. The settling times in that work are read as 10.6 s and 9.8 s for fractional order proportional integral derivative (FOPID) controller and fuzzy logic controller (FLC) respectively. In our work, the settling times are 0.2 s for speed and 0.12 s for torque in *M*-based control and 0.52 s and 0.53 s in *f*-based control for speed and torque respectively.

In terms of scalability, the modular nature of PV arrays and inverter capacity allows for flexible system sizing depending on local load requirements. Maintenance needs are modest – primarily involving periodic panel cleaning and occasional inspection of electronic components. Unlike diesel generators, PV systems offer quiet operation, zero emissions, and reduced supply chain dependency for fuel.

Deployment in remote areas may face challenges such as limited technical workforce, initial investment hurdles, and transportation logistics. However, the simplicity of the modulation index-based speed control approach ensures lower computational overhead and reduced controller complexity, making it more adaptable for areas with limited technical support. Additionally, advancements in local assembly and training programs for solar

technicians have continued to improve the long-term sustainability of such solutions in rural contexts.

CONCLUSION

This paper aimed to develop MPPT based PV fed electromechanical load for maximum exploitation purposes in rural sustainable development. The fundamental idea behind the proposal has been constant speed operation of the induction motor, even under PSC, to run some usual rural loads like tube well, plough, water pumps, and grinding machines etc. Any excess PV power from the motor drive has been used for heating or lightening load placed at the output of the boost converter. The motor load should be given priority to maintain constant speed if PV output decreases due to PSC since the drop in speed during harvesting by the motor is not desirable. However, reduced power across resistive load results in a decreased heating and dimming of lights which are not sensitive in terms of their criticality for household use.

The comprehensive model incorporates an MPPT algorithm, boost converter, PWM inverter and *M*-based and *f*-based scalar motor control system without the constant *V/f* constraint. It has been observed that *M*-based control is faster (settling time of 0.2 s and 0.12 s in N_r and T_r, respectively) and presents less oscillations in the speed output while *f*-based control is slower (settling time of >0.5 s in N_r and T_r) and less sensitive to torque changes at speed transition time. Due to the independent *V* and *f* nature, when *f* increases to increase the speed, torque decreases instantly and then increases again to regulate the speed and vice versa. This phenomenon causes substantial oscillations in the motor output in *f*-based control which would not be there even for a vector control. When the boost converter is also connected parallel to the motor drive, speed control and MPPT at PV output are achieved successfully with an accurate V_o of 2300 V as specified during the converter design process. Finally, the PSC condition is applied by reducing the irradiance from 1000 W/m^2 to 500 W/m^2 to check the output at both loads. Motor undergoes slight oscillations but reverts to N_{ref} successfully, while only the power across the converter output is reduced shown by V_o of 1629 V. The load priority is established solely by the optimum values of the controller and filter gains without the requirement of explicit scheduling algorithms to get ease of implementation.

The presented work is appealing to energy and power enterprises in developing countries for economic growth and for achieving sustainable development goals **[34]**, **[35]**. The system is fed purely with renewable energy, enabling the least operational cost to meet the current technological demands in rural areas. This research work can be extended to the analysis of the power balance between the drive and converter load under different PSC and N_{ref} values. In that case, power drawn by the motor and converter would not be equal to the PV power under MPPT because there will be harmonic loss as well which is a function of motor speed and irradiance **[36]**, **[37]**. This loss minimization requires adaptive gain scheduling and/or active filter tuning by careful control system design and parametric optimization to ensure even higher throughput and noise-free operation **[38]**.

NOMENCLATURE

C	Capacitance	[F]
f	Frequency	[Hz]
I	Current	[A]
K_p	Proportional gain	[-]
K_I	Integral gain	[-]
L	Inductance	[H]
M	Modulation index	[-]
N	Speed	[rad/sec]
P	Active power	[W]
Q	Reactive power	[VAR]

S	Apparent power	[VA]
T	Torque	[Nm]
V	Voltage	[V]

Greek letters

Φ	Phase	[°]

Subscripts and superscripts

abc	phases a, b, c
c	carrier
DC	direct current
I	integral
L	load
o	output
P	proportional
R	rotor
ref	reference
sc	short circuit
sh	shunt

Abbreviations

FLC	Fuzzy Logic Control
FOPID	Fractional Order Proportional Integral Derivative Control
FOC	Field Oriented Control
IGBT	Insulated Gate Bipolar Transistor
LCL	Inductor-Capacitor-Inductor
LMI	Linear Matrix Inequality
LQR	Linear Quadratic Regulator
MPPT	Maximum Power Point Tracking
PI	Proportional Integral
PSC	Partial Shading Condition
PV	Photovoltaic
PWM	Pulse Width Modulation
RES	Renewable Energy Sources
SS	Subsystem
THD	Total Harmonic Distortion

REFERENCES

1. T. Hák, S. Janoušková, and B. Moldan, "Sustainable Development Goals: A need for relevant indicators," Ecol. Indic., vol. 60, pp. 565-573, 2016, https://doi.org/10.1016/j.ecolind.2015.08.003.
2. T. Güney, "Renewable energy, non-renewable energy and sustainable development," Int. J. Sustain. Dev. World Ecol., vol. 26, no. 5, pp. 389-397, 2019, https://doi.org/10.1080/13504509.2019.1595214.
3. F. Chien, "The mediating role of energy efficiency on the relationship between sharing economy benefits and sustainable development goals (Case of China)," J. Innov. Knowl., vol. 7, no. 4, p. 100270, 2022, https://doi.org/10.1016/j.jik.2022.100270.
4. S. A. R. Khan, Z. Yu, A. Belhadi, and A. Mardani, "Investigating the effects of renewable energy on international trade and environmental quality," J. Environ. Manage., vol. 272, p. 111089, 2020, https://doi.org/10.1016/j.jenvman.2020.111089.

5. W. H. Organization, "Review of evidence on health aspects of air pollution: REVIHAAP project: technical report," World Health Organization. Regional Office for Europe, 2021.
6. X. Xu, Z. Wei, Q. Ji, C. Wang, and G. Gao, "Global renewable energy development: Influencing factors, trend predictions and countermeasures," Resour. Policy, vol. 63, p. 101470, 2019, https://doi.org/10.1016/j.resourpol.2019.101470.
7. J. Lowitzsch, C. E. Hoicka, and F. J. van Tulder, "Renewable energy communities under the 2019 European Clean Energy Package-Governance model for the energy clusters of the future?," Renew. Sustain. Energy Rev., vol. 122, p. 109489, 2020, https://doi.org/10.1016/j.rser.2019.109489.
8. P. K. Pathak and A. K. Yadav, "Design of battery charging circuit through intelligent MPPT using SPV system," Sol. Energy, vol. 178, pp. 79-89, 2019, https://doi.org/10.1016/j.solener.2018.12.018.
9. H. Wang, Z. Lei, X. Zhang, B. Zhou, and J. Peng, "A review of deep learning for renewable energy forecasting," Energy Convers. Manag., vol. 198, p. 111799, 2019, https://doi.org/10.1016/j.enconman.2019.111799.
10. B. Yang et al., "Comprehensive overview of maximum power point tracking algorithms of PV systems under partial shading condition," J. Clean. Prod., vol. 268, p. 121983, 2020, https://doi.org/10.1016/j.jclepro.2020.121983.
11. A. Vinayagam, A. Aziz, P. M. Balasubramaniyam, J. Chandran, V. Veerasamy, and A. Gargoom, "Harmonics assessment and mitigation in a photovoltaic integrated network," Sustain. Energy, Grids Networks, vol. 20, p. 100264, 2019, https://doi.org/10.1016/j.segan.2019.100264.
12. G. S. Krishna and T. Moger, "Improved SuDoKu reconfiguration technique for total-cross-tied PV array to enhance maximum power under partial shading conditions," Renew. Sustain. Energy Rev., vol. 109, pp. 333-348, 2019, https://doi.org/10.1016/j.rser.2019.04.037.
13. N. N. Nam, N. D. Nguyen, C. Yoon, M. Choi, and Y. Il Lee, "Voltage sensorless model predictive control for a grid-connected inverter with LCL filter," IEEE Trans. Ind. Electron., vol. 69, no. 1, pp. 740-751, 2021, https://doi.org/10.1109/TIE.2021.3050395.
14. A. Narendra, N. N. Venkataramana, A. K. Panda, N. Tiwary, and A. Kumar, "A Single-Stage SPV-Fed Reduced Switching Inverter-Based Sensorless Speed Control of IM for Water Pumping Applications," Int. Trans. Electr. Energy Syst., vol. 2022, 2022, https://doi.org/10.1155/2022/3805791.
15. B. P. Rachaputi, J. Rathinadurai Louis, and M. Sridharan, "Solar photovoltaic array fed single-stage sensorless vector control of induction motor drive for water pumping applications," Int. J. Energy Environ. Eng., pp. 1-18, 2022, https://doi.org/10.1007/s40095-022-00540-2.
16. M. Mounira and C. Djamila, "A new approach of robust speed-sensorless control of doubly fed induction motor fed by photovoltaic solar panel," Int. J. Power Electron. Drive Syst., vol. 14, no. 1, p. 153, 2023, https://doi.org/10.11591/ijpeds.v14.i1.pp153-166.
17. G. Kohlrusz and D. Fodor, "Comparison of scalar and vector control strategies of induction motors," Hungarian J. Ind. Chem., pp. 265-270, 2011.
18. V. G. BT, "Comparison between direct and indirect field oriented control of induction motor," Int. J. Eng. Trends Technol, vol. 43, no. 6, pp. 364-369, 2017, https://doi.org/10.14445/22315381/IJETT-V43P260.
19. Y. Rajbhandari et al., "Load prioritization technique to guarantee the continuous electric supply for essential loads in rural microgrids," Int. J. Electr. Power Energy Syst., vol. 134, p. 107398, 2022, https://doi.org/10.1016/j.ijepes.2021.107398.
20. M. Anthony et al., "Autonomous fuzzy controller design for the utilization of hybrid PV-wind energy resources in demand side management environment," Electronics, vol. 10, no. 14, p. 1618, 2021, https://doi.org/10.3390/electronics10141618.

21. P. Rathod, S. Bhuyan, and S. Mishra, "Power management system using modified control strategy in hybrid renewable generation system connected to grid," Int. J. Renew. Energy Res., vol. 11, no. 3, pp. 1189-1205, 2021.
22. M. Srikanth, B. Pakkiraiah, P. Upadhyay, and S. T. Kalyani, "Dual-Mode Photovoltaic Bidirectional Inverter Operation for Seamless Power Transfer to DC and AC Loads with the Grid Interface," Int. J. Photoenergy, vol. 2019, 2019, https://doi.org/10.1155/2019/8498435.
23. P. K. Pathak, A. K. Yadav, and P. A. Alvi, "A state-of-the-art review on shading mitigation techniques in solar photovoltaics via meta-heuristic approach," Neural Comput. Appl., pp. 1-39, 2022, https://doi.org/10.1007/s00521-021-06586-3.
24. P. P. Singh, S. Das, F. Wen, I. Palu, A. K. Singh, and P. Thakur, "Multi-objective planning of electric vehicles charging in distribution system considering priority-based vehicle-to-grid scheduling," Swarm Evol. Comput., p. 101234, 2023, https://doi.org/10.1016/j.swevo.2023.101234.
25. T. A. H. Alghamdi, O. T. E. Abdusalam, F. Anayi, and M. Packianather, "An artificial neural network based harmonic distortions estimator for grid-connected power converter-based applications," Ain Shams Eng. J., p. 101916, 2022, https://doi.org/10.1016/j.asej.2022.101916.
26. M. S. Choudhary et al., "Solar powered space vector pulse width modulation based induction motor drive for industry applications," Bull. Electr. Eng. Informatics, vol. 11, no. 4, pp. 1828-1836, 2022, https://doi.org/10.11591/eei.v11i4.3023.
27. A. Kumar and R. Agarwal, "Assessment of Solar Inverter-Powered Induction Motor Effectiveness in Partially Shaded Conditions," in International Conference on Green Energy and Sustainable Technology, 2023, pp. 281-304, https://doi.org/10.1007/978-981-96-1012-9_19.
28. N. I. Nahin, S. P. Biswas, M. K. Hosain, M. R. Islam, S. Mondal, and A. Fekih, "Advanced model predictive control strategy for solar PV fed induction motor drives," in 2023 IEEE International Conference on Applied Superconductivity and Electromagnetic Devices (ASEMD), 2023, pp. 1-2, https://doi.org/10.1109/ASEMD59061.2023.10368910.
29. M. Ciobotaru, R. Teodorescu, and F. Blaabjerg, "Control of single-stage single-phase PV inverter," Epe J., vol. 16, no. 3, pp. 20-26, 2006, https://doi.org/10.1080/09398368.2006.11463624.
30. P. K. Pathak, A. K. Yadav, S. Padmanaban, and P. A. Alvi, "Design of Robust Multi-Rating Battery Charger for Charging Station of Electric Vehicles via Solar PV System," Electr. Power Components Syst., vol. 50, no. 14-15, pp. 751-761, 2022, https://doi.org/10.1080/15325008.2022.2139870.
31. A. Feroz Mirza, M. Mansoor, Q. Ling, M. I. Khan, and O. M. Aldossary, "Advanced variable step size incremental conductance MPPT for a standalone PV system utilizing a GA-tuned PID controller," Energies, vol. 13, no. 16, p. 4153, 2020, https://doi.org/10.3390/en13164153.
32. S. Shelar, D. Bankar, and S. Bakre, "Review of revisions of IEEE 519 Standard on Power System Harmonics (1981 to 2022)," in 2024 21st International Conference on Harmonics and Quality of Power (ICHQP), 2024, pp. 415-420, https://doi.org/10.1109/ICHQP61174.2024.10768696.
33. S. Chandrasekaran, S. Durairaj, and S. Padmavathi, "A performance improvement of the fuzzy controller-based multi-level inverter-fed three-phase induction motor with enhanced time and speed of response," J. Electr. Eng. Technol., vol. 16, pp. 1131-1141, 2021, https://doi.org/10.1007/s42835-020-00649-6.
34. Y. A. Fatimah, K. Govindan, R. Murniningsih, and A. Setiawan, "Industry 4.0 based sustainable circular economy approach for smart waste management system to achieve sustainable development goals: A case study of Indonesia," J. Clean. Prod., vol. 269, p. 122263, 2020, https://doi.org/10.1016/j.jclepro.2020.122263.

35. J. Gunawan, P. Permatasari, and C. Tilt, "Sustainable development goal disclosures: Do they support responsible consumption and production?," J. Clean. Prod., vol. 246, p. 118989, 2020, https://doi.org/10.1016/j.jclepro.2019.118989.
36. M. N. Bhukya, V. R. Kota, and S. R. Depuru, "A simple, efficient, and novel standalone photovoltaic inverter configuration with reduced harmonic distortion," IEEE Access, vol. 7, pp. 43831-43845, 2019, https://doi.org/10.1109/ACCESS.2019.2902979.
37. M. S. Ramkumar, S. Sakthikumar, A. Amudha, and G. Emayavaramban, "Three Phase Reduction of Inter Harmonic Analysis of PV-MPPT Grid Connected Systems under Partial Shading Conditions," in 2022 International Conference on Edge Computing and Applications (ICECAA), 2022, pp. 768-776, https://doi.org/10.1109/ICECAA55415.2022.9936399.
38. H. Singh, S. Gupta, and A. Gupta, "Implementation of an anti-windup control under partial shading for a photovoltaic grid interfaced system," in IOP Conference Series: Earth and Environmental Science, 2023, vol. 1110, no. 1, p. 12082, https://doi.org/10.1088/1755-1315/1110/1/012082.

Paper submitted: 15.01.2025
Paper revised: 26.06.2025
Paper accepted: 30.06.2025